

Control of chemically driven convective dissolution by differential diffusion effects

M. Jotkar ^{*}, A. De Wit [†], and L. Rongy [‡]

*Nonlinear Physical Chemistry Unit, Faculté des Sciences, Université libre de Bruxelles (ULB),
Campus Plaine, C.P. 231, 1050 Brussels, Belgium*



(Received 23 December 2020; accepted 5 May 2021; published 27 May 2021)

Chemically driven convective dissolution can occur upon reaction of a dissolving species in a host phase when the chemical reaction destabilizes an otherwise stable density stratification. An $A + B \rightarrow C$ reaction is known to trigger such convection when, upon dissolution into the host solution, A reacts with B present in the solution to produce a sufficiently denser product C. We study numerically the effect of differential diffusion on such a chemically driven convective dynamics. We show that below the reaction front either double-diffusive or diffusive-layer convection can arise, modifying the local Rayleigh-Taylor instability. When B diffuses faster than C, the density profile contains a local maximum at the reaction front, followed by a local minimum below it. A double-diffusive instability can develop below the reaction front, accelerating the convective dynamics and thereby enhancing the dissolution rate of A into the host phase. Conversely, when B diffuses slower than C, the density profile exhibits a local maximum below the reaction front and diffusive-layer convection modes stabilize the dynamics compared to the equal diffusivity case. When B and C diffuse at equal rates but faster than A, the convective dynamics is accelerated with respect to the equal diffusivity case.

DOI: [10.1103/PhysRevFluids.6.053504](https://doi.org/10.1103/PhysRevFluids.6.053504)

I. INTRODUCTION

When, upon dissolution of a species into a host phase, the density increases monotonically along the gravity field, the situation is stable with respect to buoyancy-driven convection, and transport is governed by diffusion. Chemical reactions in the host phase can nevertheless induce convection in such systems by creating unstable nonmonotonic density profiles with a local maximum in the gravity field [1–10]. A classical Rayleigh-Taylor instability then occurs locally where a denser zone lies on top of a less dense one. This so-called chemically driven convective dissolution (CDCD) can be of significant relevance for various technological applications, where it is desirable to either promote or hinder convection [1–4, 11].

In particular, an $A + B \rightarrow C$ reaction is known to induce CDCD when the sole dissolution of species A in the host phase creates a stable density profile but its subsequent reaction with B initially present in the host solution produces locally a sufficiently denser solution of product C [9]. While the nonreactive dynamics is controlled by diffusion alone, convective fingering can be triggered above a critical value of the difference between B and C contributions to the solution density and the dissolution rate of species A into the host phase can be enhanced [9]. More generally, any solid dissolving in a liquid from below or most gases except CO_2 dissolving in a liquid from the top give

^{*}Present address: Universidad Politécnica de Madrid, ETSI Caminos, Canales y Puertos, Madrid, Spain; mamta.jotkar@upm.es

[†]Anne.De.Wit@ulb.be

[‡]Laurence.Rongy@ulb.be

rise to situations that are prone to be destabilized by CDCD. The alkaline oxidation of glucose by oxygen with methylene blue as catalyst and indicator, also referred to as the “blue bottle reaction,” is another example [2–4].

While few studies have considered CDCD, there exists a vast literature on convective dissolution with nonreactive unstable density profiles in relevance to CO_2 capture and sequestration techniques [12]. In that case, the dissolving species (CO_2) increases the density of the host phase (e.g., brine) upon dissolution from above, which eventually gives rise to a buoyancy-driven fingering instability referred to as dissolution-driven convection [13–19]. This convective instability can be further intensified with the help of chemical reactions [5–8,20–31]. More specifically, an $A + B \rightarrow C$ reaction can accelerate or slow down dissolution-driven convection depending on the relative contribution to density of each of the species present in the host solution [7,22,23,25,29–31].

The diffusion coefficients of the chemical species can also play an important role in controlling the dynamics. The various reaction-diffusion density profiles that can develop after the dissolution of a species A in a host phase containing B when the solutes of an $A + B \rightarrow C$ reaction diffuse at different rates have been theoretically classified for both cases where the nonreactive counterpart is stable and unstable [6].

The unstable case has received far more attention. For such systems, differential diffusivity effects have been evidenced experimentally [21,25] and investigated theoretically [8,30,32–34]. It was shown that, when the species diffuse at different rates, additional dynamics occur below the reaction front. Specifically, a double-diffusive (DD) instability can develop when a less dense solution of a slow-diffusing solute locally overlies a denser solution of a fast-diffusing solute. Diffusive-layer convection (DLC) with two separate zones of convection and antennae-shaped fingers occurs when a less dense solution containing a fast-diffusing solute is layered over a denser solution of a slow-diffusing solute [30,33,34]. Theoretical studies have shown that differential diffusion affects the growth rate in the linear regime [8] and the onset time of dissolution-driven convection can be reduced or increased [32,34], as can the dissolution flux of A [34].

The role of differential diffusion has been much less investigated for CDCD. It has been shown theoretically that double-diffusive mechanisms can further destabilize chemically driven convection when B diffuses faster than C [8,32,33]. However, several open questions remain.

More precisely, the impact of differential diffusion on the nonlinear convective dynamics, the temporal evolution of the dissolution flux of species A into the host phase, its asymptotic value, and the onset time for convection are not yet known. The case where B and C diffuse at equal rates but different from that of A also remains to be investigated.

Following this motivation, we numerically study the effect of differential diffusion on CDCD. We focus here on initially stable density stratifications where the dissolving phase A is introduced from above and decreases the density of the host phase. Upon dissolution into the host phase, A then reacts with B to produce C via an $A + B \rightarrow C$ reaction. We study the effect of varying the diffusivities of B and C on the nonlinear chemically driven convective dynamics and on the dissolution flux of species A.

The article is organized as follows. We explain the numerical model in Sec. II and classify the density profiles in Sec. III. We analyze the case where B diffuses faster than C in Sec. IV, followed by the case of B diffusing slower than C in Sec. V. The case where B and C diffuse at the same rate but different from that of A is presented in Sec. VI. In Sec. VII, we quantify the onset time and asymptotic flux of dissolving A. The highlights of this work are discussed in Sec. VIII.

II. PROBLEM FORMULATION

Following previous theoretical works [7,9,31], we consider a homogeneous, isotropic porous medium where two partially miscible phases are initially separated by a horizontal interface. The gravitational field g acts along the vertical z' . The contact line between the two phases is oriented along the horizontal x' axis at $z' = 0$. Phase A dissolves into the host phase containing a reactant B

with an initial concentration B_0 . Upon dissolution, A reacts with B via a bimolecular $A + B \rightarrow C$ reaction to generate C. Here we will consider that all the species contribute to the density of the host phase and diffuse at different rates. The scenario where A decreases the density of the host solution when dissolving from above is analogous to the one where A increases the density when introduced from below [9]. Both these situations correspond, in the absence of reactions, to stable density stratifications where density increases along the gravity field. The host phase extends from $x' = 0$ to $x' = L'$ in the horizontal x' direction and from $z' = 0$ to $z' = H'$ in the vertical z' direction (primes denote dimensional quantities).

The solute concentrations, time, spatial coordinates, and velocity are nondimensionalized using the solubility A_0 of A in the host solution, the chemical reaction time scale, the diffusive length scale based on the diffusivity of species A, and the Darcy velocity scale [9].

The dimensionless reaction-diffusion-convection equations for the concentrations of species A, B, and C are

$$\frac{\partial A}{\partial t} + (\mathbf{u} \cdot \nabla)A = \nabla^2 A - AB, \quad (1a)$$

$$\frac{\partial B}{\partial t} + (\mathbf{u} \cdot \nabla)B = \delta_B \nabla^2 B - AB, \quad (1b)$$

$$\frac{\partial C}{\partial t} + (\mathbf{u} \cdot \nabla)C = \delta_C \nabla^2 C + AB, \quad (1c)$$

where $\mathbf{u} = (u, v)$ is the two-dimensional velocity field, $\delta_B = D_B/D_A$, and $\delta_C = D_C/D_A$, with D_A , D_B , and D_C the diffusivities of species A, B, and C, respectively.

The evolution equation for the velocity field in porous media is Darcy's law

$$\nabla p = -\mathbf{u} + \rho \mathbf{e}_z, \quad (2)$$

with p the dimensionless pressure and \mathbf{e}_z the unit vector along the gravity field. A linear equation of state is used for the dimensionless density ρ of the host solution

$$\rho = R_A A + R_B B + R_C C, \quad (3)$$

where the Rayleigh numbers R_i ($i = A, B, C$) are defined as

$$R_i = \frac{\alpha_i A_0 g \kappa}{\phi \nu \sqrt{D_A q A_0}}, \quad (4)$$

with $\alpha_i = \frac{1}{\rho_0} \frac{\partial \rho'}{\partial c'_i}$ the solutal expansion coefficient of species i , ρ_0 the dimensional density of the solvent, κ the permeability, q the kinetic constant of the reaction, and ν the kinematic viscosity of the solvent. The Rayleigh number R_i quantifies the contribution to density of species i [9]. It is to be noted that this definition is different from the classical one used in the literature [18]. We chose here this particular definition of Rayleigh numbers in order to make our results independent of the domain height H .

Most studies on convective dissolution have considered the cases where all species increase the density ($R_i > 0$). Here, we analyze the case $R_A < 0$ and $R_{B,C} > 0$ such that A decreases the density of the host phase while B and C increase it. In the absence of reactions, the density stratification is stable and exhibits a diffusive profile when A dissolves from the top.

Periodic boundary conditions are imposed at the lateral sides, no vertical flow and no flux conditions are used for A, B, and C at the bottom while, at the top interface, no vertical flow and no flux conditions are used for B and C along with $A = 1$ (assuming local chemical equilibrium between the dissolving phase and the host phase at the interface). We use the following initial conditions:

$$A(x, z = 0, t = 0) = 1 + \epsilon \cdot \text{rand}(x); \quad A(x, z > 0, t = 0) = 0, \quad (5a)$$

$$B(x, z, t = 0) = \beta, \quad (5b)$$

$$C(x, z, t = 0) = 0, \quad (5c)$$

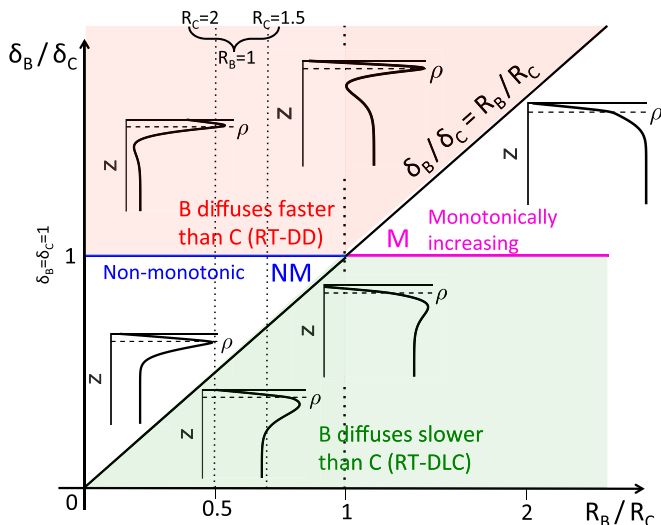


FIG. 1. Classification of the RD density profiles $\rho(z)$ in the $(R_B/R_C, \delta_B/\delta_C)$ space for $R_A = -1$ and $R_C > 0$ with horizontal dashed black lines on the density profiles representing the location of the reaction front: regimes NM (nonmonotonic with maximum at the reaction front), M (monotonically increasing), RT-DD indicated by the red region (maximum at the reaction front followed by a minimum below), and RT-DLC indicated by the green region (maximum below the reaction front). Adapted from Ref. [6]. The equal diffusivity cases [9] with C denser than B (indicated by the blue solid line) and C less dense than B (indicated by the pink solid line) are similar to regimes NM and M, respectively. Note that the profiles are sketched for $\beta = 1$ but a similar classification can be made for different β as well.

where $\beta = B_0/A_0$ is the ratio of the initial concentration B_0 of B and the solubility A_0 . Perturbations with amplitude $\epsilon = 10^{-3}$ are introduced in Eq. (5a) to trigger the instability while $\text{rand}(x)$ varies randomly between -1 and 1 [35,36].

The problem depends on six parameters: δ_B , δ_C , R_A , R_B , R_C , and β . We concentrate here on differential diffusivity effects and vary δ_B , δ_C , R_B , and R_C for $R_A = -1$ and $\beta = 1$. The computational domain width used is $L = 3072$, while a height $H = 2048$ is used when $R_C = 1.5$ and $H = 4096$ when $R_C = 2$. Further details on the numerics can be found in Refs. [7,37].

III. CLASSIFICATION OF THE DENSITY PROFILES

To understand the potential effect of differential diffusion on the CDCD dynamics, we first classify the reaction-diffusion (RD) density profiles $\rho(z, t)$ in the $(R_B/R_C, \delta_B/\delta_C)$ parameter space (see Fig. 1). The profiles obtained by numerical integration of RD equations (Eq. (1)) with $\mathbf{u} = 0$ are shown at a given time. The exact time is not important as the qualitative features of the RD profiles remain the same over time.

We recall that, in the absence of reactions, the density profiles are monotonically increasing along gravity because the dissolving species A decreases the density of the host solution ($R_A < 0$). In the presence of an $A + B \rightarrow C$ reaction, the density profile can remain monotonically increasing or become nonmonotonic (Fig. 1). In an equal diffusivity scenario, the density profile exhibits a local maximum at the reaction front when the product C is denser than reactant B ($R_B/R_C < 1$, blue line in Fig. 1). When the difference $\Delta R_{CB} = R_C - R_B$ in the contribution of C and B to the solution density is above a certain critical value, a region of denser solution locally overlies a less dense one, which triggers a Rayleigh-Taylor (RT) instability [9]. For $\beta = 1$ chosen here, this critical

value is $\Delta R_{CB} = 0.35$. Note that ΔR_{CB} was used to classify the density profiles for equal diffusion coefficients in Ref. [9], whereas we classify the dynamics here as a function of R_B/R_C to demonstrate the effect of δ_B/δ_C [6].

When B diffuses sufficiently faster than C, it creates a local depletion below the reaction front so that the density profiles exhibit a local maximum at the reaction front followed by a local minimum below it. In that case, it gives rise to a region with a less dense solution locally lying on top of a denser one with the bottom part of the solution containing the fast-diffusing solute B. This promotes double-diffusive convection that couples with the local RT instability (red region in Fig. 1: RT-DD dynamics when $\delta_B/\delta_C > \max[1, R_B/R_C]$).

Conversely, when B diffuses slower than C, the local maximum can occur below the reaction front because of the presence of fast-diffusing C in this region. Between the reaction front and the position where the density is maximum, a less dense solution of fast-diffusing C locally overlies a denser solution of the slow-diffusing B leading to diffusive-layer convection influencing the RT instability (green region in Fig. 1: RT-DLC mechanism when $\delta_B/\delta_C < \min[1, R_B/R_C]$).

In summary, four distinct regimes can be identified based on the RD density profiles. The dynamics in regime NM with nonmonotonic density profiles and regime M with monotonically increasing density profiles are qualitatively similar to the equal diffusivity scenarios when C is denser than B and when C is equally dense or less dense than B, respectively. Here, we concentrate therefore on the red (RT-DD) and green (RT-DLC) regimes of Fig. 1 where differential diffusion leads to additional convective dynamics below the reaction front. In the following sections, we study the nonlinear convective dynamics for specific cases in the RT-DD and RT-DLC regions.

IV. ACCELERATED CONVECTIVE DYNAMICS

We first study the nonlinear convective dynamics in the red (RT-DD) regime of Fig. 1 when B diffuses faster than C.

Let us first consider a case where C is equally dense as B ($R_B/R_C = 1$). If $\delta_B = \delta_C$, the density profile is monotonically increasing along gravity and the situation is stable (qualitatively similar to the pink line M in Fig. 1). However, if B diffuses faster than C, a nonmonotonic density profile develops because of differential diffusion with a maximum at the reaction front followed by a minimum below it. At the reaction front, B is readily consumed by the reaction to produce the slow-diffusing solute C. The extremum triggers a local RT instability while the stratification of the slow-diffusing C above the fast-diffusing B promotes DD convection that works cooperatively with the local RT instability. The density fields at different times are shown for $\delta_B/\delta_C = 3$ (red RT-DD regime of Fig. 1) in the top line of Fig. 2 with $R_B = R_C = 1$. The zone above the reaction front is stable as the density increases along the gravity field (see the density profile enclosed in the first panel). However, after an initial diffusive transient (not shown here), a fingering instability with a uniform wavelength is triggered below the reaction front. Thereafter, the fingers merge, increasing the wavelength, and then gradually sink towards the bottom, after which an asymptotic limit is reached.

When C is denser than B ($R_B/R_C < 1$), the equal diffusivity scenario exhibits nonmonotonic density profiles (blue line NM in Fig. 1) that become unstable above the critical difference $\Delta R_{CB} = 0.35$ (for $\beta = 1$ chosen here) [9]. The density fields for $R_B = 1$, $\delta_B/\delta_C = 3$ are shown for $R_C = 1.5$ and $R_C = 2$ in the middle and bottom line of Fig. 2, respectively. Both cases are above $\Delta R_{CB} = 0.35$ such that they are already unstable for equal diffusion coefficients. If now B diffuses faster than C, the RT-DD interplay is promoted, similar to the dynamics when $R_B = R_C = 1$. However, the dynamics depends on the relative value of the density at the interface and in the bulk. For equal diffusion coefficients, the interface value of the density is equal to that far away in the bulk when the difference $\Delta R_{CB} = R_C - R_B$ is equal to $-R_A/\beta$ [9]. This value cannot be computed analytically for $\delta_B/\delta_C \neq 1$, but we estimate that this happens here between $R_C = 1.5$ and 2. The interface value of density is indeed smaller than its bulk value for $R_C = 1.5$ but larger than its bulk value for $R_C = 2$.

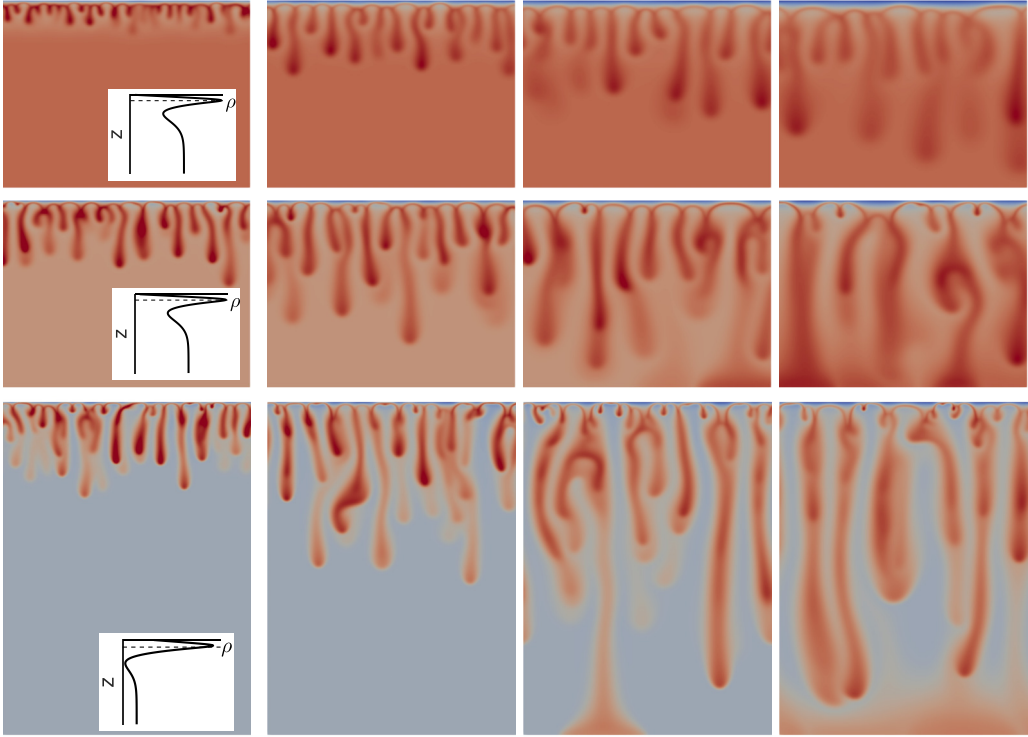


FIG. 2. Density ρ fields at times $t = 5000$, 10000 , 20000 , and 30000 from left to right in the RT-DD regime indicated in red in Fig. 1 with $\delta_C = 1$, $\delta_B = 3$, $R_B = 1$ for $R_C = 1$ (top), $R_C = 1.5$ (middle), and $R_C = 2$ (bottom). Typical 1D RD density profiles are enclosed in the first panel. Density scales between its minimum (blue) and maximum (red) values in each line.

As a consequence, the RT dynamics is stronger for the latter. This explains why fingers extend on a larger vertical zone for $R_C = 2$ than for $R_C = 1.5$ at similar times (Fig. 2). Thus, for a given diffusivity ratio $\delta_B/\delta_C = 3$, when C is denser than B , DD effects are at play but, when R_B/R_C is decreased, the overall dynamics becomes dominated by the RT instability.

Figure 3 shows the concentration fields of A , B , and C and the reaction rate AB corresponding to the density field shown in the top line of Fig. 2 for $R_B = 1$ and $R_C = 1$ at $t = 30000$. The fingering pattern is mainly due to the denser product C sinking towards the bottom and being replaced by the fast-diffusing B from the bulk, while the dissolving species A is readily consumed by the reaction

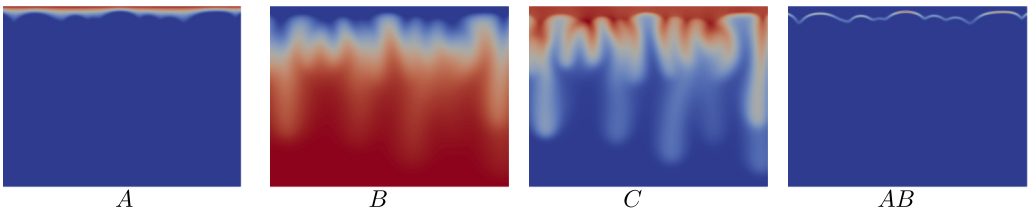


FIG. 3. Concentration fields of A , B , and C and the distribution of the reaction rate AB corresponding to the density field shown in the top line of Fig. 2 at $t = 30000$. Concentration and reaction rate scale between their minimum (blue) and maximum (red) values.

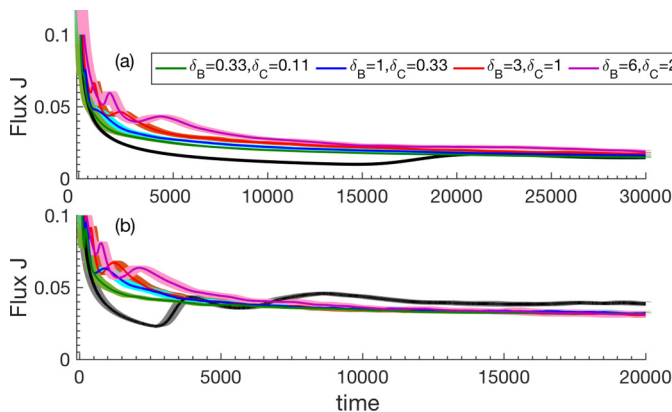


FIG. 4. Temporal evolution of the dissolution flux J for different δ_B, δ_C indicated in the inset for the destabilizing RT-DD cases with $\delta_B/\delta_C = 3, R_B = 1$, and (a) $R_C = 1.5$; (b) $R_C = 2$. Solid black curves correspond to the cases with equal diffusion coefficients.

as soon as it enters the host phase. The reaction rate AB is maximum along the tips of the fingers formed by A .

With an objective of determining the efficiency of a given convective dissolution process, we compute the dissolution flux J , defined as

$$J = -\frac{1}{L} \int_0^L \frac{\partial A}{\partial z} \Big|_{z=0} dx, \quad (6)$$

where L is the domain width.

Figure 4 shows the temporal evolution of the dissolution flux J for different absolute values of diffusion coefficients (δ_B, δ_C) with $\delta_B/\delta_C = 3$. One curve represents the average over 15 realizations with different initial noise of a given amplitude in Eq. (5a). The lighter areas around the curves represent the variability due to the random noise on the initial condition. Initially, the flux J decreases as $1/\sqrt{t}$ in the diffusive regime. Soon after the onset of the fingering instability, J increases above the diffusive trend, features one or two peaks, and eventually fluctuates around an asymptotic value J^* . Qualitatively, this behavior is similar to the nonreactive scenario with $R_A > 0$ [16] and to the reactive ones for equal diffusion coefficients with $R_A > 0$ [7,31] or $R_A < 0$ [9].

Note that the equal diffusivity $\delta_B = \delta_C = 1$ cases indicated by the solid black curves are different when $R_C = 1.5$ and $R_C = 2$. The latter develops stronger convective motions since the product C is denser and the RT instability is stronger. When B diffuses faster than C , the RT-DD interplay causes an earlier departure of J from the diffusive regime, followed by an earlier occurrence of the peaks and J reaches the asymptotic regime sooner. The overall dynamics is accelerated due to the fast-diffusing solute B being more readily available at the reaction front for consumption by the reaction. When $R_C = 2$, the asymptotic values J^* are, however, slightly lower than those for $\delta_B = \delta_C = 1$. This can be explained by the fact that, when R_C increases, the interface value of the density increases and the local RT instability becomes stronger. It seems that, for such a case, increasing the diffusivity ratio only acts to weaken this instability. For a given $\delta_B/\delta_C = 3$, various absolute values of diffusivities δ_B and δ_C also impact the temporal evolution of the flux J (Fig. 4). The larger δ_B and δ_C , the most efficient the double diffusive effect and the larger the asymptotic flux J^* .

The space-time plots of density at location $z = 128$ below the interface are shown in Fig. 5 for $R_B = 1$ with $R_C = 1.5$ (left) and $R_C = 2$ (right), where the middle line corresponds to the equal diffusivity $\delta_B = \delta_C = 1$ cases. We chose the location $z = 128$ such that it is sufficiently below the stable boundary layer to follow the convective dynamics. The accelerated dynamics with stronger

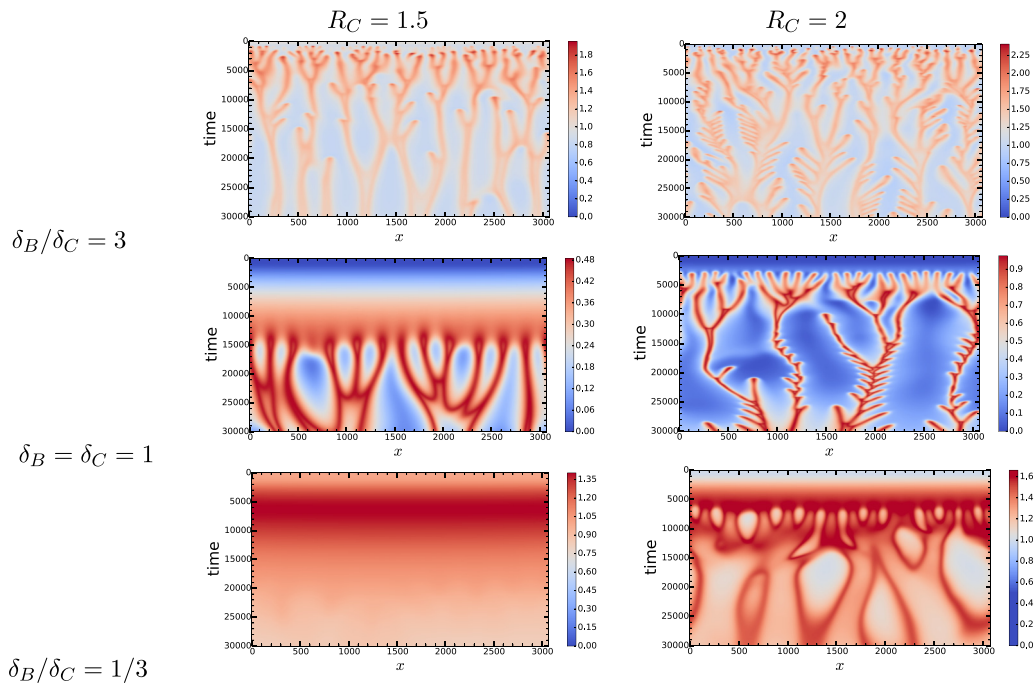


FIG. 5. Space-time plots of the density computed at $z = 128$ below the interface for $R_B = 1$ with $R_C = 1.5$ (left) and $R_C = 2$ (right). Destabilizing RT-DD cases with $\delta_B/\delta_C = 3$ (top) and stabilizing RT-DLC cases with $\delta_B/\delta_C = 1/3$ (bottom) are compared to the equal diffusivity $\delta_B = \delta_C = 1$ cases (middle).

convective motion due to the RT-DD mechanism can be seen here in the top line when B diffuses faster than C.

V. STABILIZING CONVECTIVE DYNAMICS

Let us now consider the green regime (RT-DLC) of Fig. 1, when B diffuses slower than C and $R_B/R_C > \delta_B/\delta_C$.

The density profiles contain a local maximum below the reaction front. A less dense solution of the fast-diffusing solute C overlies a denser solution of the slow-diffusing B. This promotes DLC below the reaction front that couples with the local RT instability generated by the unstable decreasing density profile below the maximum. The density fields for $R_C = 1.5$ (top) and 2 (bottom) with $\delta_B/\delta_C = 1/3$ and $R_B = 1$ are shown in Fig. 6. For both cases, we observe two distinct zones: the part above the reaction front dominated by diffusion and the one below it where fingers are formed. The interface between the two zones remains flat up to large times and the fingers do not interact with each other significantly. At the reaction front where C is generated by the reaction, the slow-diffusing solute B from the bulk is scarcely available for consumption by the reaction. For $R_C = 1.5$ in the top line of Fig. 6, the fingers formed remain localized due to the weak RT instability and small intensity of the local maximum in density. Eventually, they merge but continue to be localized. For $R_C = 2$, in the bottom line of Fig. 6, the RT instability is stronger causing the fingers to merge gradually and move towards the bottom relatively faster. Fingers feature the classical antenna sides typical of DLC modes [38]. As explained in the previous section, the space-time plots of density at location $z = 128$ below the interface are shown in Fig. 5 for $R_B = 1$ with $R_C = 1.5$ (left) and $R_C = 2$ (right). The weak convective motion due to the RT-DLC mechanism can be seen here

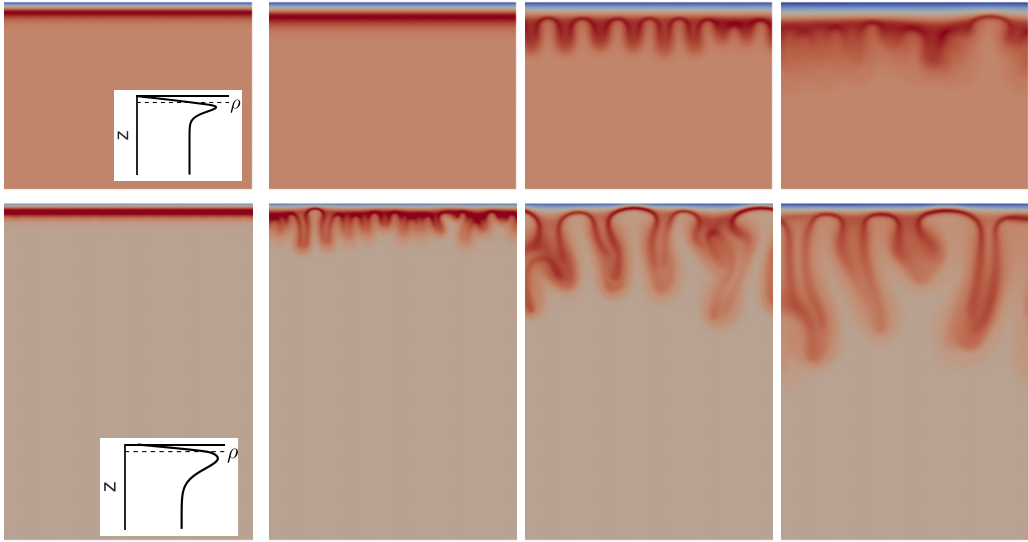


FIG. 6. Density ρ fields at times $t = 5000, 10000, 20000,$ and 30000 from left to right in the RT-DLC regime indicated in green in Fig. 1 with $\delta_C = 1, \delta_B = 1/3, R_B = 1$ for $R_C = 1.5$ (top) and $R_C = 2$ (bottom). Typical 1D RD density profiles are enclosed in the first panel. Density scales between its minimum (blue) and maximum (red) values in each line.

in the bottom line. The formation of the fingering pattern is delayed significantly compared to the RT-DD and equal diffusivity cases.

Figure 7 shows the temporal evolution of the dissolution flux of A for different absolute values of diffusion coefficients (δ_B, δ_C) with $\delta_B/\delta_C = 1/3$. We observe that, when B diffuses slower than C for $R_C = 1.5$, the flux J continues to follow the diffusive scaling whereas, for $R_C = 2$, the onset of the convective instability is delayed significantly in most cases. Once again, for a given $\delta_B/\delta_C = 1/3$, various absolute values of diffusion coefficients δ_B and δ_C also impact the temporal evolution of the flux J . The smaller the values of δ_B and δ_C for a fixed ratio, the stronger the RT instability.

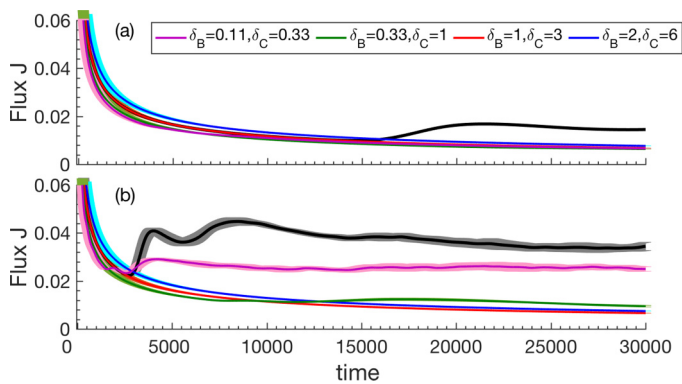


FIG. 7. Temporal evolution of the dissolution flux J for different diffusivities indicated in the inset for the stabilizing RT-DLC cases with $\delta_B/\delta_C = 1/3, R_B = 1,$ and (a) $R_C = 1.5;$ (b) $R_C = 2$. Solid black curves correspond to the cases with equal diffusion coefficients.

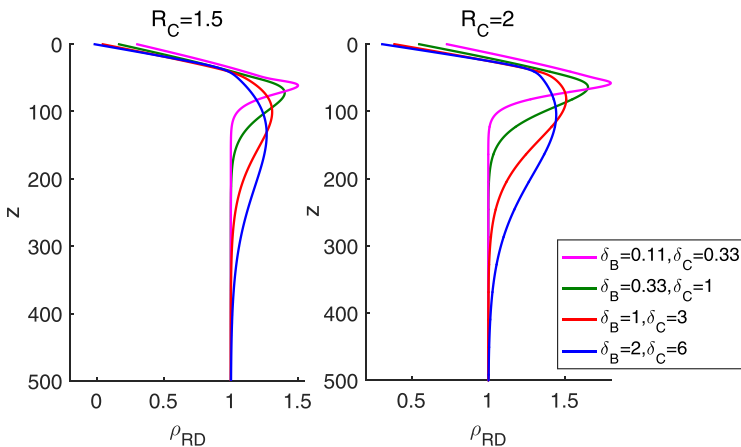


FIG. 8. RD density profiles for different diffusion coefficients (δ_B , δ_C) indicated in the inset for the stabilizing RT-DLC cases $\delta_B/\delta_C = 1/3$ with $R_B = 1$ and (left) $R_C = 1.5$; (right) $R_C = 2$.

To corroborate this point, we have plotted RD density profiles for different diffusion coefficients (δ_B , δ_C) for a given $\delta_B/\delta_C = 1/3$ in Fig. 8. When the diffusion coefficients are smaller, the density profiles exhibit steeper slopes below the local maximum that, in turn, strengthen the RT instability for a given ratio $\delta_B/\delta_C = 1/3$.

Thus we have shown that when B diffuses slower than C the dynamics is substantially stabilized compared to the equal diffusivity case, through RT-DLC interplay.

VI. CONVECTIVE DYNAMICS WHEN B AND C DIFFUSE AT THE SAME RATE

Let us now consider the cases where B and C diffuse at the same rate but differently from A.

We recall that, for $\delta_B/\delta_C = 1$, the density profiles are nonmonotonic when C is denser than B, with the local maximum occurring at the reaction front (blue NM line in Fig. 1). Figure 9 shows the

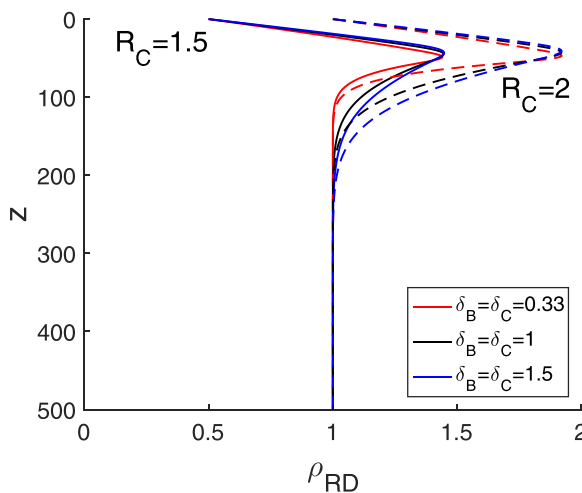


FIG. 9. RD density profiles for different diffusion coefficients (δ_B , δ_C) indicated in the inset for $\delta_B/\delta_C = 1$ with $R_B = 1$ for $R_C = 1.5$ (solid curves) and $R_C = 2$ (dashed curves).

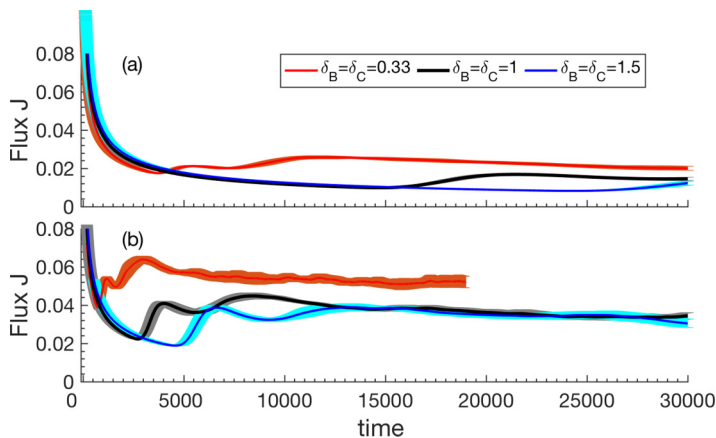


FIG. 10. Temporal evolution of the dissolution flux J when B and C diffuse at equal rates $\delta_B/\delta_C = 1$ for different values of the diffusivities indicated in the inset with $R_B = 1$ and (a) $R_C = 1.5$; (b) $R_C = 2$.

RD density profiles for different diffusion coefficients (δ_B , δ_C) such that $\delta_B/\delta_C = 1$. When B and C diffuse at an equal rate but faster than A ($\delta_B = \delta_C > 1$) the slope below the local maximum becomes less steep. Consequently, this weakens the local RT instability. Figure 10 shows the dissolution fluxes for $R_B = 1$ with $R_C = 1.5$ and 2 and various values of $\delta_B = \delta_C$. For both cases, when B and C diffuse at the same rate but faster than A, the dynamics is less unstable with smaller asymptotic fluxes J^* and later departure of flux J from the diffusive trend. On the other hand, when B and C diffuse at an equal rate but slower than A ($\delta_B = \delta_C < 1$), the density profile exhibits a steeper slope below the local maximum (Fig. 9) and the local RT instability becomes stronger as seen by the earlier departure of flux from the diffusive limit and higher values of J^* (Fig. 10).

This shows that, even when B and C diffuse at the same rate but different from the rate of A, the dissolution flux can be altered.

VII. ONSET TIMES AND ASYMPTOTIC FLUXES

To further quantify the effect of differential diffusion on chemically driven convective dissolution, we now study the onset time for convection and the asymptotic flux for different values of δ_B and δ_C .

The onset time t_0 for convection is defined here based on the magnitude of the velocity field $U^2(t) = \int_0^H \int_0^L [u^2(x, z, t) + v^2(x, z, t)] dx dz$. Initially, U^2 decreases up to a minimum value. At the onset time t_0 , it begins to grow due to the convective instability [7]. Figure 11 shows the onset times t_0 for all the diffusivities studied here when C is denser than B, i.e., for $R_B = 1$ with $R_C = 1.5$ and 2. The equal diffusivity cases are indicated by the horizontal dashed lines. The values of t_0 can be reduced up to two orders of magnitude for $\delta_B/\delta_C > 1$ (red RT-DD regime in Fig. 1) compared to the equal diffusivity scenario thanks to the RT-DD interplay. On the other hand, when $\delta_B/\delta_C < 1$, the onset times t_0 can be up to two orders of magnitude larger. We also observe that, for a given ratio of δ_B/δ_C , the absolute values of the diffusion coefficients δ_B and δ_C also impact the onset times t_0 .

We now quantify the asymptotic flux J^* as a function of δ_B/δ_C in Fig. 12. For a given $R_B = 1$, the values of J^* are larger than that for the equal diffusivity case when B diffuses faster than C ($\delta_B/\delta_C > 1$) with $R_C = 1.5$. However, we note that, for $R_C = 2$, the J^* values are slightly lower. As discussed earlier, this might be due to the relative values of the densities at the interface and far away in the bulk. When B diffuses slower than C ($\delta_B/\delta_C < 1$), the values of J^* are lower than the equal

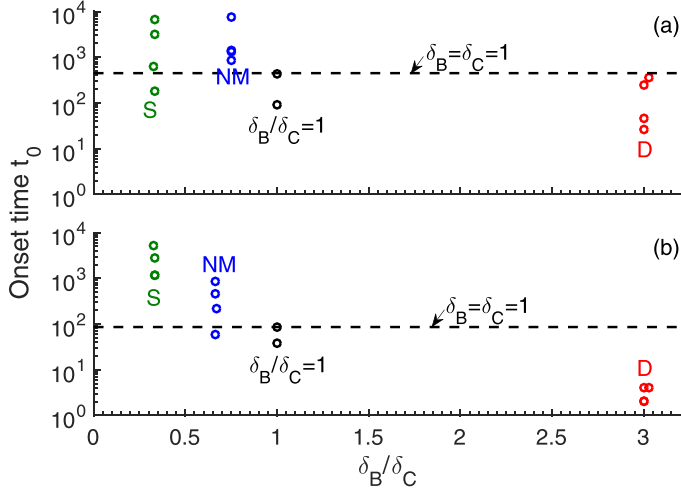


FIG. 11. Onset time t_0 for different diffusivity ratios δ_B/δ_C and $R_B = 1$ when (a) $R_C = 1.5$ and (b) $R_C = 2$. Dashed lines represent the equal diffusivity cases. For a given ratio δ_B/δ_C , various combinations of absolute values of diffusion coefficients (δ_B , δ_C) are used. The letters S and D refer to stabilizing RT-DLC and destabilizing RT-DD cases, respectively. NM stands for nonmonotonic as in Fig. 1.

diffusion cases for both $R_C = 1.5$ and 2. Here again, we observe that, for a given ratio of diffusivity δ_B/δ_C , changing the absolute values of the diffusion coefficients δ_B and δ_C also alters the J^* values.

To summarize, we have shown that differential diffusion has a significant impact on the storage rates directly related to the dissolution flux of A. The dynamics can be accelerated with the help of the RT-DD interplay when B diffuses faster than C and slowed down via RT-DLC mechanisms when B diffuses slower than C.

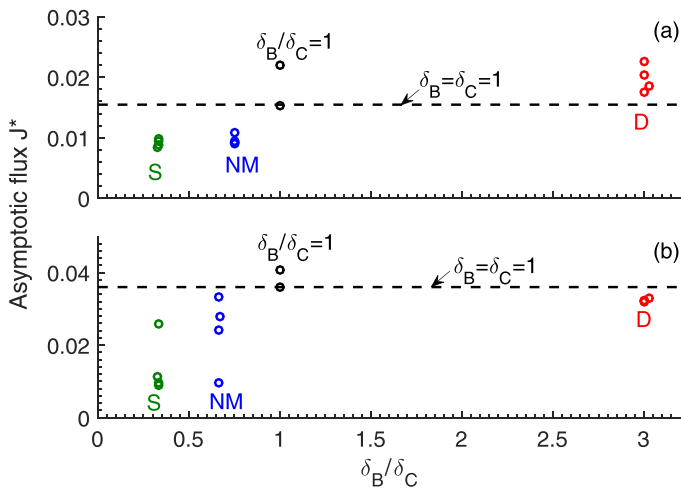


FIG. 12. Asymptotic flux J^* for different diffusivity ratios δ_B/δ_C and $R_B = 1$ when (a) $R_C = 1.5$ and (b) $R_C = 2$. Same conventions are used as in Fig. 11.

VIII. CONCLUSION

We have numerically studied the role of differential diffusion on chemically driven convective dissolution (CDCD) dynamics when the dissolving species A introduced from above decreases the density of the host phase upon dissolution. This case is analogous to dissolution from below of a species A that would increase the density upon dissolution. In the absence of reactions, the situation is buoyantly stable and diffusion is the only transport mechanism. By modifying the density profile in the host solution, an $A + B \rightarrow C$ reaction can induce buoyancy-driven convective fingering beyond a certain critical difference in the density contribution between C and B [9]. We have investigated here the role of differential diffusion of the solutes A, B, and C on CDCD.

When B diffuses faster than C, the density profiles contain a local maximum at the reaction front, followed by a local minimum below it. This gives rise to a RT-DD interplay, where double-diffusive convection reinforces the Rayleigh-Taylor instability. This contributes to the reduction of the onset times for convection up to two orders of magnitude and a larger dissolution flux in general.

On the other hand, when B diffuses slower than C, the density profiles contain a local maximum below the reaction front which leads to two distinct zones: the diffusion-dominated one above the reaction front and RT-DLC fingering below. The interface between the two zones remains flat up to very large times inhibiting the interaction between fingers. In some cases, the dissolution flux even continues to follow the diffusive scaling. This has a stabilizing effect with lower asymptotic fluxes and up to two orders of magnitude increase in the onset times.

When B and C diffuse at the same rate but faster (slower) than A, the dynamics can be accelerated (slowed down). Although the morphology of the convective patterns is determined by the relative ratio of δ_B/δ_C and R_B/R_C , we observe that, for a given ratio δ_B/δ_C , the absolute values of diffusion coefficients also impact the values of onset times and asymptotic fluxes.

In conclusion, differential diffusion can alter the dynamics of chemically driven convective dissolution, modify the dissolution rate and even induce convection in otherwise stable situations. Our results are relevant for various geological applications or engineering setups that involve nonreactive stable density stratifications where transport can be enhanced by reaction-induced convection.

ACKNOWLEDGMENTS

We thank B. Knaepen and V. Loodts for their help and support concerning the YALES2 code. We gratefully acknowledge the financial support from the Fondation ULB and from the FRS-FNRS PDR CONTROL project.

-
- [1] O. Citri, M. L. Kagan, R. Kosloff, and D. Avnir, Evolution of chemically induced unstable density gradients near horizontal reactive interfaces, *Langmuir* **6**, 559 (1990).
 - [2] A. J. Pons, F. Sagués, M. A. Bees, and P. Graae Sørensen, Pattern formation in the methylene-blue-glucose system, *J. Phys. Chem. B* **104**, 2251 (2000).
 - [3] M. A. Bees, A. J. Pons, P. G. Sørensen, and F. Sagués, Chemoconvection: A chemically driven hydrodynamic instability, *J. Chem. Phys.* **114**, 1932 (2001).
 - [4] A. J. Pons, O. Batiste, and M. A. Bees, Nonlinear chemoconvection in the methylene-blue-glucose system: Two-dimensional shallow layers, *Phys. Rev. E* **78**, 016316 (2008).
 - [5] V. Loodts, L. Rongy, and A. De Wit, Chemical control of dissolution-driven convection in partially miscible systems: Theoretical classification, *Phys. Chem. Chem. Phys.* **17**, 29814 (2015).
 - [6] V. Loodts, P. M. J. Trevelyan, L. Rongy, and A. De Wit, Density profiles around $A+B \rightarrow C$ reaction-diffusion fronts in partially miscible systems: A general classification, *Phys. Rev. E* **94**, 043115 (2016).
 - [7] V. Loodts, B. Knaepen, L. Rongy, and A. De Wit, Enhanced steady-state dissolution flux in reactive convective dissolution, *Phys. Chem. Chem. Phys.* **19**, 18565 (2017).

- [8] M. C. Kim and S. S. S. Cardoso, Diffusivity ratio effect on the onset of the buoyancy-driven instability of an $A+B \rightarrow C$ chemical reaction system in a Hele-Shaw cell: Asymptotic and linear stability analyses, *Phys. Fluids* **30**, 094102 (2018).
- [9] M. Jotkar, L. Rongy, and A. De Wit, Chemically-driven convective dissolution, *Phys. Chem. Chem. Phys.* **21**, 19054 (2019).
- [10] A. De Wit, Chemo-hydrodynamic patterns and instabilities, *Annu. Rev. Fluid Mech.* **52**, 531 (2020).
- [11] E. L. Paul, V. Atiemo-Obeng, and S. M. Kresta, *Handbook of Industrial Mixing: Science and Practice* (Wiley, New York, 2003).
- [12] Intergovernmental Panel on Climate Change (IPCC) special report on *Carbon Dioxide Capture and Storage* (Cambridge University Press, New York, 2005).
- [13] G. S. Pau, J. B. Bell, K. Pruess, A. S. Almgren, M. J. Lijewski, and K. Zhang, High-resolution simulation and characterization of density-driven flow in CO_2 storage in saline aquifers, *Adv. Water Resour.* **33**, 443 (2010).
- [14] M. T. Elenius and K. Johannsen, On the time scales of nonlinear instability in miscible displacement porous media flow, *Comput. Geosci.* **16**, 901 (2012).
- [15] A. C. Slim, M. M. Bandi, J. C. Miller, and L. Mahadevan, Dissolution-driven convection in a Hele-Shaw cell, *Phys. Fluids* **25**, 024101 (2013).
- [16] A. C. Slim, Solutal-convection regimes in a two-dimensional porous medium, *J. Fluid Mech.* **741**, 461 (2014).
- [17] H. E. Huppert and J. A. Neufeld, The fluid mechanics of carbon dioxide sequestration, *Annu. Rev. Fluid Mech.* **46**, 255 (2014).
- [18] H. Emami-Meybodi, H. Hassanzadeh, C. P. Green, and J. Ennis-King, Convective dissolution of CO_2 in saline aquifers: Progress in modeling and experiments, *Int. J. Greenhouse Gas Control* **40**, 238 (2015).
- [19] C. Thomas, S. Dehaeck, and A. De Wit, Convective dissolution of CO_2 in water and salt solutions, *Int. J. Greenhouse Gas Control* **72**, 105 (2018).
- [20] J. Ennis-King and L. Paterson, Coupling of geochemical reactions and convective mixing in the long-term geological storage of carbon dioxide, *Int. J. Greenhouse Gas Control* **1**, 86 (2007).
- [21] C. Wylock, A. Rednikov, B. Haut, and P. Colinet, Nonmonotonic Rayleigh-Taylor instabilities driven by gas-liquid CO_2 chemisorption, *J. Phys. Chem. B* **118**, 11323 (2014).
- [22] M. A. Budroni, L. A. Riolfo, L. Lemaigre, F. Rossi, M. Rustici, and A. De Wit, Chemical control of hydrodynamic instabilities in partially miscible two-layer systems, *J. Phys. Chem. Lett.* **5**, 875 (2014).
- [23] V. Loodts, C. Thomas, L. Rongy, and A. De Wit, Control of Convective Dissolution by Chemical Reactions: General Classification and Application to CO_2 Dissolution in Reactive Aqueous Solutions, *Phys. Rev. Lett.* **113**, 114501 (2014).
- [24] S. S. S. Cardoso and J. T. H. Andres, Geochemistry of silicate-rich rocks can curtail spreading of carbon dioxide in subsurface aquifers, *Nat. Commun.* **5**, 5743 (2014).
- [25] C. Thomas, V. Loodts, L. Rongy, and A. De Wit, Convective dissolution of CO_2 in reactive alkaline solutions: Active role of spectator ions, *Int. J. Greenhouse Gas Control* **53**, 230 (2016).
- [26] I. Cherezov and S. S. S. Cardoso, Acceleration of convective dissolution by chemical reaction in a Hele-Shaw cell, *Phys. Chem. Chem. Phys.* **18**, 23727 (2016).
- [27] C. Wylock, A. Rednikov, P. Colinet, and B. Haut, Experimental and numerical analysis of buoyancy-induced instability during CO_2 absorption in NaHCO_3 - Na_2CO_3 aqueous solutions, *Chem. Eng. Sci.* **157**, 232 (2017).
- [28] P. Ghoshal, M. C. Kim, and S. S. S. Cardoso, Reactive-convective dissolution in a porous medium: The storage of carbon dioxide in saline aquifers, *Phys. Chem. Chem. Phys.* **19**, 644 (2017).
- [29] M. A. Budroni, C. Thomas, and A. De Wit, Chemical control of dissolution-driven convection in partially miscible systems: Nonlinear simulations and experiments, *Phys. Chem. Chem. Phys.* **19**, 7936 (2017).
- [30] V. Loodts, H. Saghou, B. Knaepen, L. Rongy, and A. De Wit, Differential diffusivity effects in reactive convective dissolution, *Fluids* **3**, 83 (2018).
- [31] M. Jotkar, A. De Wit, and L. Rongy, Enhanced convective dissolution due to an $A+B \rightarrow C$ reaction: Control of the non-linear dynamics via solutal density contributions, *Phys. Chem. Chem. Phys.* **21**, 6432 (2019).

- [32] M. C. Kim and S. S. S. Cardoso, Diffusivity ratio effect on the onset of the buoyancy-driven instability of an $A+B \rightarrow C$ chemical reaction system in a Hele-Shaw cell: Numerical simulations and comparison with experiments, [Phys. Fluids **31**, 084101 \(2019\)](#).
- [33] T. Lei and K. H. Luo, Differential diffusion effects on density-driven instability of reactive flows in porous media, [Phys. Rev. Fluids **5**, 033903 \(2020\)](#).
- [34] M. Jotkar, L. Rongy, and A. De Wit, Reactive convective dissolution with differential diffusivities: Nonlinear simulations of onset times and asymptotic fluxes, [Phys. Rev. Fluids **5**, 104502 \(2020\)](#).
- [35] M. Bestehorn and A. Firoozabadi, Effect of fluctuations on the onset of density-driven convection in porous media, [Phys. Fluids **24**, 114102 \(2012\)](#).
- [36] N. Tilton, D. Daniel, and A. Riaz, The initial transient period of gravitationally unstable diffusive boundary layers developing in porous media, [Phys. Fluids **25**, 092107 \(2013\)](#).
- [37] V. Loodts, Ph.D. thesis, Université libre de Bruxelles, 2016.
- [38] J. Carballido-Landeira, P. M. J. Trevelyan, C. Almarcha, and A. De Wit, Mixed-mode instability of a miscible interface due to coupling between Rayleigh-Taylor and double-diffusive convective modes, [Phys. Fluids **25**, 024107 \(2013\)](#).